PCCP

PAPER

View Article Online
View Journal | View Issue

Cite this: *Phys. Chem. Chem. Phys.*, 2015, **17**, 32183

Photoinduced water splitting *via* benzoquinone and semiquinone sensitisation

Tolga N. V. Karsili,* Deniz Tuna,† Johannes Ehrmaier and Wolfgang Domcke

Received 2nd July 2015,
Accepted 29th September 2015

DOI: 10.1039/c5cp03831f

www.rsc.org/pccp

The splitting of water into H$^\bullet$ and OH$^\bullet$ radicals by sensitisation of a redox-active chromophore with sunlight may eventually become a viable way of producing unlimited, clean and sustainable energy. In this work, we explore the possibility of photo-oxidation of water *via* sensitisation of benzoquinone with ultraviolet (UV) light in the hydrogen-bonded complex of benzoquinone with a single water molecule. Using state-of-the-art quantum chemical calculations, the mechanisms of electron/proton transfer reactions between photoexcited benzoquinone and water are characterised. In the benzoquinone–H_2O complex, photoexcitation of the chromophore leads to the population of locally excited $\pi\pi^*$ and $n\pi^*$ singlet states, which are coupled to hitherto unknown charge-transfer states. In the latter, an electron is transferred from the oxygen atom of the water molecule to the lowest π^* orbital of benzoquinone. These charge-separated states drive the transfer of a proton from the water molecule to the carbonyl acceptor site, yielding the semiquinone–OH$^\bullet$ biradical. Upon absorption of a second UV photon, the semiquinone radical may undergo O–H bond fission, which generates an H$^\bullet$ radical and restores the benzoquinone photocatalyst. Our computational results shed light on long-standing questions regarding the nature of the photoreactive electronic states in the aqueous photochemistry of benzoquinone.

1. Introduction

The UV mediated photosynthesis of H_2O and CO_2 into glucose and O_2 in plant leaves is crucial for sustaining life on earth.[1] Much of this photochemistry occurs within photosystems I and II and includes the photo-reduction of plastoquinone to plastoquinol. The present work focusses on the excited-state reactivity of the simplest quinone, *p*-benzoquinone (BQ), with H_2O in the BQ–H_2O hydrogen-bonded complex in the context to the lessons learnt from recent explorations of the photochemistry of the pyridine–H_2O and acridine–H_2O complexes.[2–4] BQ is a photoactive chromophore that exhibits a large redox potential. It is therefore widely used as a hydrogen-accepting reagent in organic syntheses and serves as a dehydration agent.[5] Such redox activity also makes BQ an efficient precursor in many organic reactions – notably the Diels–Alder reaction.[6] Experimentally, the redox potential of BQ has been measured to increase upon photoexcitation at selected wavelengths – strongly improving its hydrogen accepting ability.[7] This property of BQ is of particular interest for the current work in which the excited-state H-atom transfer reaction leading to the oxidation of H_2O *via* BQ sensitization is explored.

The photoinduced reactivity of quinones with the solvent H_2O has attracted vast attention – with studies spanning about half a century (1950–2000). In these investigations, the lack of knowledge of the precise reaction mechanisms has caused much controversy concerning the finer details of the photoreactivity of quinones with H_2O. Here, we can survey only a subset of the extensive literature in this field to date. Most investigations of the photochemistry of quinones have been conducted in acidic (pH $\sim$ 3) or neutral (pH $\sim$ 7) aqueous media and large yields for hydrogenated (quinol) photoproducts with equimolar concentrations have been reported.[7–11] Formation of these products was postulated to proceed *via* a photoreaction in a triplet excited electronic state that is formed *via* intersystem crossing (ISC) from an initially excited state of singlet multiplicity. This is a reasonable postulation since such carbonyl group containing systems generally possess high quantum yields for ISC.[12,13] In the case of BQ, the majority photoproducts include semiquinone (BQH$^\bullet$) and hydroquinone (BQH_2) – formed, respectively, *via* single or double hydrogenation of BQ, as well as additional minor products resulting from chain reactions of BQ and BQH_2 with OH$^\bullet$ radicals to form *ortho*-hydroxy substituted adducts (*i.e.* benzene-1,2,4-triol and 2-hydroxy-1,4-benzoquinone). It has been suggested that the OH$^\bullet$ radical formed upon photo-oxidation of H_2O by BQ is not free in solution, but is instead complexed with the resulting BQH$^\bullet$ radical – forming a biradical.[14] This would explain why the yields of the above described chain reactions involving the OH$^\bullet$ radical are relatively low.

Department of Chemistry, Technische Universität München, D-85747 Garching, Germany. E-mail: tolga.karsili@tum.de; Tel: +49 (0)89 289 13608

† Present address: Max-Planck-Institut für Kohlenforschung, D-45470 Mülheim an der Ruhr, Germany.

Variations in the solvent environment influence the photochemistry of quinones and have therefore attracted much attention.[15–17] In alcoholic solvents, photo-excited quinones are also capable of oxidation – yielding hydrogenated products formed *via* excited-state hydrogen transfer. The rate constant for hydrogen transfer was observed to increase upon increasing the aliphatic chain length – which may reflect a greater stabilization of the resulting RO$^\bullet$ radical *via* an increased +I inductive effect. In contrast to quinones in H_2O, the photoreactivity of quinones with *tert*-butanol is substantially lower and, in addition, the H-atom abstracted by the quinone moiety is exclusively from a C–H bond in the α position to the O–H group. This implies that the resulting tertiary radical intermediate is more stable than the *tert*-RO$^\bullet$ radical which is formed by H-atom abstraction from the OH moiety. In general, the observed rate constants associated with photoreactions of quinones with alcohols are significantly lower than those for quinones with water.

Direct measurements of the lifetimes of intermediate species associated with such photo-oxidation reactions have received less attention when compared with ground-state reactivity experiments. Studies of the photoreactivity of quinones in aqueous solution using, for example, ultrafast transient pump–probe spectroscopy are essential for determining the timescales on which the hydrogen-transfer reaction occurs. Ronfard-Haret *et al.*[18] and Moore *et al.*[19] performed time-resolved experiments using, respectively, nanosecond flash photolysis and nanosecond resonance Raman spectroscopy – both of which report the appearance of a long-lived semiquinone radical absorption. Such studies cannot give, however, lifetime information for the non-adiabatic excited-state processes involved in the hydrogen-transfer reaction – which are typically ultrafast, that is, proceed on femtosecond timescales. By analogy with other hydrogen-bonded systems that undergo excited-state hydrogen transfer, it is expected that low-energy conical intersections (CIs) govern the ultrafast non-adiabatic processes intrinsic to the observed photoreactions.[20–22] CIs are ubiquitous in many of the ultrafast processes in photochemistry and the pronounced anharmonicity of their potential-energy (PE) surfaces as well as the strong nonadiabatic couplings at CIs are important in driving and controlling photoinduced reactions.[23–27]

In view of the lack of time-resolved studies with femtosecond resolution for photoreactions of quinones with hydrogen-donating solvents, first-principles theoretical investigations are essential for the development of a complete mechanistic understanding of these excited-state photoreactions. Here we report the use of *ab initio* electronic-structure theory to identify the excited electronic states involved in these photoreactions and to establish essential topographic properties of the excited-state PE surfaces involved in the oxidation of H_2O *via* BQ sensitization. In the present study we have chosen the BQ–H_2O hydrogen bonded complex as a prototypical model system for the exploration of the basic photoinduced reaction mechanisms with accurate first-principles methods. We have explored the excited-state photoreactivity of the BQ–H_2O complex in the singlet and triplet manifolds in an attempt to develop an understanding of the intrinsic hydrogen-transfer mechanisms involved in the photoredox reaction of BQ with H_2O. The theoretical study of spin-forbidden intersystem-crossing (ISC) processes as such is beyond the scope of the present work.

2. Computational methodology

The ground-state equilibrium geometry was optimized in both C_1 and C_s symmetries using Møller-Plesset second-order perturbation theory (MP2),[28] coupled with Dunning's correlation consistent double-ζ basis set (cc-pVDZ).[29] Vertical excitation energies and oscillator strengths were calculated using the complete-active-space second-order perturbation theory (CASPT2)[30] method and the second-order algebraic diagrammatic construction (ADC(2)) method.[31] The reaction path for H-atom transfer in the electronic ground state was calculated at the MP2 level of theory using the bond length of the hydrogen-bonded OH group of water as the driving coordinate. The S_0 energy was scanned along $R_{O(2)–H(3)}$ (henceforth simply $R_{O–H}$), fixing the O–H bond length at selected values and, at each step, allowing all other internal degrees of freedom to relax to the minimum-energy conformation. The energies of the $^1n\pi^*$, $^3n\pi^*$, $^1\pi\pi^*$, and $^3\pi\pi^*$ excited states along the relaxed ground-state path were computed using the ADC(2) method. Relaxed scans along $R_{O–H}$ were also computed in the $^1\pi\pi^*$ and $^3\pi\pi^*$ excited states of charge-transfer character (*vide infra*) using the ADC(2) method in the excited-state geometry optimizations. In this case, the energies of the electronic ground state and the $^1n\pi^*$ and $^3n\pi^*$ states were computed at the relaxed geometries of the $^1\pi\pi^*$ or $^3\pi\pi^*$ states using the MP2 and ADC(2) methods, respectively. To avoid convergence problems, it was necessary to freeze the distance between the donor and acceptor oxygen atoms whilst scanning the relaxed $^1\pi\pi^*$ scan for $R_{O–H} > 1.4$ Å. Where the calculation of relaxed scans was not possible due to a failure of excited-state geometry optimization, an approximate reaction path was constructed by linear interpolation in internal coordinates between initial and final geometries.

The CASPT2 calculations for BQ–H_2O were based on a complete-active-space self-consistent-field (CASSCF) reference wave function. Test calculations with varying active spaces were carried out in order to find the active space which describes all significant effects of the ground and excited states in a balanced way whilst minimizing computational expense and convergence problems. The optimal active space for bare BQ was found to comprise of 12 electrons in 10 orbitals (12/10). The active orbital space consisted of four occupied π, four unoccupied π* orbitals and two occupied n orbitals, comprising two a′ and eight a″ orbitals. In the case of BQ–H_2O, the optimal active space consisted of 14 electrons distributed into 12 orbitals (14/12) – comprising four π and four π* orbitals, two $2p_y$ lone pairs centered on each of the oxygen atom of BQ, the $2p_x$ orbital centered on the oxygen atom of water and a σ* orbital localized on the O–H bond of water. In both bare BQ and the BQ–H_2O complex, the CASSCF reference wave function was computed using state-averaged orbitals. The state averaging included three $^1A'$ and $^3A'$ states as well as two $^1A''$ and $^3A''$ states.

The ground-state equilibrium geometries of $BQH^{\bullet}$ and BQH_2 were calculated using unrestricted and restricted MP2 theory, respectively. Unrelaxed (rigid-body) scans along the O–H stretching coordinates of $BQH^{\bullet}$ and BQH_2 were calculated at the CASPT2/aug-cc-pVDZ level of theory, varying the O–H bond distance and keeping all other internal degrees of freedom fixed at the MP2/cc-pVDZ equilibrium geometry of the ground state. It has been shown previously that rigid scans are a good approximation for the photodetachment of H-atoms *via* repulsive $\pi\sigma^*$ states.[46] These calculations were based on a state-averaged CASSCF reference wave function and utilized a (12/11) active space for both $BQH^{\bullet}$ and BQH_2. For $BQH^{\bullet}$, the active space consisted of four π and three π^* orbitals, the O centred $2p_y$ orbital, the O–H centred σ and σ^* orbitals and the 3s Rydberg orbital centered on the hydroxyl O atom. For BQH_2, the active space comprised three π and three π^* orbitals, two O centered $2p_x$ orbitals, the O–H centered σ and σ^* orbitals and the 3s Rydberg orbital. Augmentation of the cc-pVDZ basis set is essential for the excited states of $\pi\sigma^*$ character in $BQH^{\bullet}$ and BQH_2 and thus the aug-cc-pVDZ was applied to all atoms.[20]

All MP2 and ADC(2) calculations were undertaken with Turbomole 6.4[32] whereas the CASSCF and CASPT2 calculations were performed using Molpro 2010.1.[33]

3. Results and discussion

3.1 Ground-state minimum-energy geometry of the BQ–H_2O complex

Fig. 1(a) and (b) depict the ground-state minimum-energy geometry of the BQ–H_2O hydrogen-bonded complex optimised with, respectively, C_1 and C_s symmetry constraints. The global minimum-energy configuration in the ground electronic state is depicted in Fig. 1(a) and displays a BQ–H_2O hydrogen-bond length of 2.032 Å and a C5O4$\cdots$H3 hydrogen-bond angle of $\sim$112°. This bent hydrogen-bond geometry can be understood by recognising that the dominant hydrogen bond acceptor is the in-plane $2p_y$ non-bonding orbital localised on O(4). The C_1 optimised global minimum is calculated to be only 0.04 eV ($\sim$350 cm^{-1}) more stable than the equivalent configuration optimised with C_s symmetry constraint in which BQ and H_2O are coplanar (Fig. 1(b)). For the purposes of the present study, these subtle differences in the ground-state energy are unimportant. Since the excited-state calculations are greatly simplified in C_s symmetry, the construction of the reaction paths for H-atom transfer and the PE profiles described hereafter were carried out with C_s symmetry constraint – unless stated otherwise.

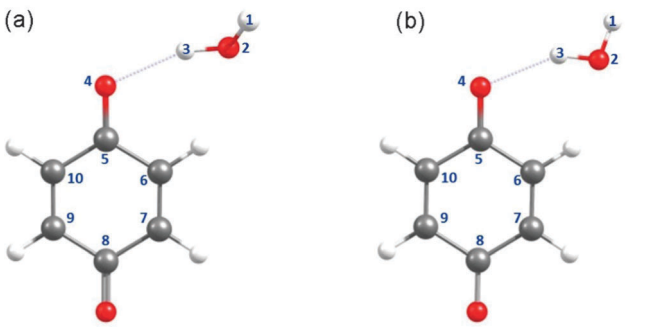

Fig. 1 Minimum-energy geometries of the BQ–H_2O complex optimised at the MP2/cc-pVDZ level with (a) C_1 and (b) C_s constrained symmetries. The free OH group in (a) is out-of-plane with respect to the aromatic ring plane. (a) Represents the global minimum-energy geometry of BQ–H_2O which is 0.04 eV (350 cm^{-1}) more stable than (b).

3.2 Vertical excitation energies and oscillator strengths

Table 1 lists the calculated vertical excitation energies and oscillator strengths associated with excitations to the low-lying electronic states of BQ and BQ–H_2O. The associated orbitals and orbital promotions for BQ and BQ–H_2O are displayed in Fig. 2.

(A) Bare BQ. The lowest vertically excited singlet states are, respectively, $^1n\pi^*$ and $^1\pi\pi^*$ in nature. The transitions to these states are electric-dipole forbidden in the D_{2h} symmetry group. The $^1\pi\pi^*$ state corresponds to the excitation from the $4a''(\pi)$ orbital to the $5a''(\pi^*)$ orbital, see Fig. 2. We note that two quasi-degenerate $^1n\pi^*$ states exist in the FC region (see Table 1). These quasi-degenerate states arise *via* electron promotion from the $2p_y$ orbitals localised on each oxygen atom to a common π^* orbital ($5a''$ in Fig. 2). In what follows we will focus solely on the lower of the two quasi-degenerate $^1n\pi^*$ states as it is sufficient to do so for the present study. As is evident from Fig. 2, the orbitals involved in the $^1n\pi^* \leftarrow S_0$ transition show poor spatial overlap, whereas the $^1\pi\pi^*$ state arises from the $5a'' \leftarrow 4a''$ excitation in which the involved orbitals (as depicted in Fig. 2) show good spatial overlap. Despite the dipole forbidden character, experiments have confirmed that both the $^1n\pi^*$ and $^1\pi\pi^*$ states exhibit appreciable absorption cross sections due to vibronic coupling with allowed electronic states.

At the ground-state minimum-energy geometry, CASSCF, CASPT2 and ADC(2) consistently predict the energetic ordering of these states to be $^1n\pi^* < {}^1\pi\pi^*$ – which is in agreement with previous experimental[34] and theoretical[35–40] findings, see Table 1. The vertical excitation energies calculated using ADC(2) and CASPT2 are, respectively, 2.72 eV and 2.47 eV for $1^1n\pi^*$ and

Table 1 Vertical excitation energies and oscillator strengths (in parentheses) of BQ and BQ–H_2O

	Vertical excitation energy/eV			
State	CASSCF/cc-pVDZ	CASPT2/cc-pVDZ	ADC(2)/cc-pVDZ	Experimental value
Benzoquinone				
$1^1n\pi^*$	3.20 (0.0)	2.47	2.72 (0.0)	2.479[34]
$2^1n\pi^*$	3.22 (0.0)	2.47	2.80 (0.0)	2.485[34]
$1^1\pi\pi^*$	4.90 (0.0)	4.30	4.83 (0.0)	4.070[34]
$2^1\pi\pi^*$	6.03 (0.0)	4.56	5.53 (0.0)	—
$1^3n\pi^*$	3.05	2.27	2.38	2.314[52]
$1^3\pi\pi^*$	3.80	3.34	3.52	—
Benzoquinone–water				
$1^1n\pi^*$	3.40 (1.1×10^{-6})	2.71	2.67 (1.7×10^{-7})	—
$2^1n\pi^*$	3.75 (2.3×10^{-7})	2.90	2.91 (1.93×10^{-6})	—
$1^1\pi\pi^*$	5.63 (0.0017)	4.34	4.68 (0.0037)	—
$2^1\pi\pi^*$	5.92 (0.0060)	4.49	5.45 (0.5486)	—
$1^3n\pi^*$	3.24	2.50	2.33	—
$1^3\pi\pi^*$	3.69	3.23	3.11	—

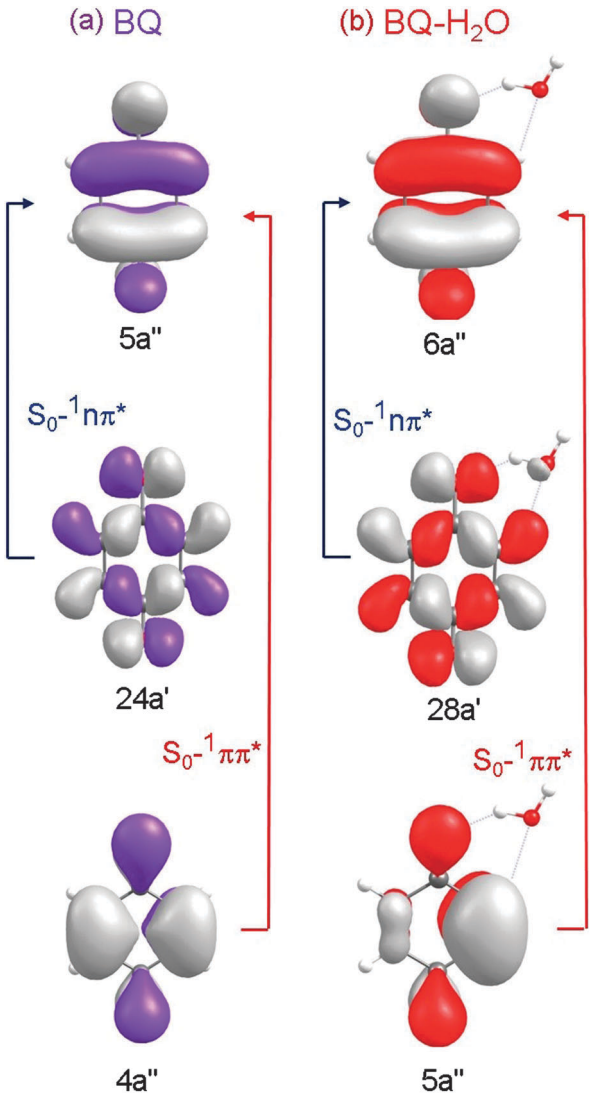

Fig. 2 Hartree–Fock orbitals and orbital promotions involved in forming the first three excited singlet states of BQ (left) and the corresponding locally excited singlet states of BQ–H_2O (right).

4.83 and 4.30 eV for $^1\pi\pi^*$ – which are close to the experimentally derived values of 2.7 eV ($^1n\pi^*$) and 4.44 eV ($^1\pi\pi^*$).[34] As is generally observed, CASPT2 tends to underestimate the energies of $\pi\pi^*$ states of aromatic systems, while ADC(2) tends to overestimate the $\pi\pi^*$ excitation energies. It is noteworthy that the comparatively inexpensive single-reference ADC(2) method returns vertical excitation energies of comparable accuracy as the multi-reference CASPT2 method.

Excitation energies of the analogous triplet states were also computed using CASSCF, CASPT2 and ADC(2). As expected, these lie lower in energy than the singlet states involving the same orbital promotions (see Fig. 2(a)). The present results are in good agreement with previous theoretical studies of the excitation energies of BQ.[36–40]

(B) BQ–H_2O complex. Table 1 also displays the calculated vertical excitation energies of the low-energy electronic states of the BQ–H_2O complex. As with bare BQ, the lowest singlet excited states of BQ–H_2O are $^1n\pi^*$ and $^1\pi\pi^*$ in nature. The calculated CASPT2 energies are, respectively, 2.71 eV and 4.34 eV. The ADC(2) vertical excitation energies agree well with those derived from CASPT2. As with bare BQ, two low-lying $n\pi^*$ states exist below the $^1\pi\pi^*$ state – but unlike BQ, the presence of a chelating H_2O molecule results in a lifting of the quasi-degeneracy such that the two $^1n\pi^*$ states are separated by 0.35 eV (*cf.* 0.02 eV for bare BQ). Analogous to BQ, the dark $^1n\pi^*$ states involve orbital promotions from the $2p_y$ lone pair localised on the O atoms to the ring centred π^* orbital. The bright $^1\pi\pi^*$ state also involves the analogous orbital promotion to that of bare BQ – *i.e.* a ring centred $\pi^* \leftarrow \pi$ excitation. In the Franck–Condon (FC) region, both $^1n\pi^*$ and $^1\pi\pi^*$ states are locally excited states of BQ – since both orbitals participating in the electron promotion are localised on BQ.

The triplet states involve the same orbital promotions as those for the analogous singlet excited configurations. The $^3\pi\pi^*$ electronic state is located at significantly lower vertical energy than the $^1\pi\pi^*$ electronic state, but still above the lowest $^1n\pi^*$ state.

3.3 Excited-state reactivity in the BQ–H_2O complex: electron-driven proton transfer

Where applicable, we refer to the atomic numberings displayed in Fig. 1 in the following description of the excited-state reactivity of the BQ–H_2O complex. Eqn (1) below represents the proposed photoinduced hydrogen-abstraction reaction in the BQ–H_2O complex to form the $BQH^\bullet$–$OH^\bullet$ biradical. Eqn (2) describes the photodissociation of the resulting $BQH^\bullet$ radical that may occur by the absorption of a second photon (*vide infra*).

$$BQ\text{–}H_2O + h\nu \rightarrow BQH^\bullet + OH^\bullet \quad (1)$$

$$BQH^\bullet + h\nu \rightarrow BQ + H^\bullet \quad (2)$$

It should be noted that BQ acts as a photobase in reaction (1), while $BQH^\bullet$ acts as a photoacid in reaction (2).

PE profiles for the S_0, $^1n\pi^*$ and $^1\pi\pi^*$ states along the O(2)–H(3) bond extension coordinate (corresponding to photoreaction (1)), in the range 1.0 Å $\geq R_{O2\text{–}H3} \geq$ 2.0 Å, are presented in Fig. 3(a). The analogous $^3n\pi^*$ and $^3\pi\pi^*$ PE profiles associated with this photoreaction are displayed in Fig. 3(b). Small values of the O–H bond length ($R_{O\text{–}H} \approx$ 1.0 Å) correspond to the equilibrium geometry of the BQ–H_2O complex, while large values of the O–H bond length ($R_{O\text{–}H} \approx$ 2.0 Å) correspond to $BQH^\bullet$–$OH^\bullet$ biradicals. The curves in Fig. 3(a) and (b) show the energy profiles of two different minimum-energy reaction paths. The energy of the electronic ground state along the reaction path optimized in the ground state is given by the full black circles on the lower left-hand side. The energies of the locally excited states along this reaction path are represented by the blue ($n\pi^*$) and red ($\pi\pi^*$) open circles. For clarity, the energy profiles of the locally excited state are shown only for $R_{O\text{–}H} <$ 1.1 Å (vertical dashed lines in Fig. 3(a) and (b)). The energy of the lowest $\pi\pi^*$ state of charge-transfer (CT) character along the reaction path optimized in this excited state is given by the full red circles in Fig. 3(a) and (b). The energies of the S_0 state and the $n\pi^*$ excited state along this reaction path are given by the

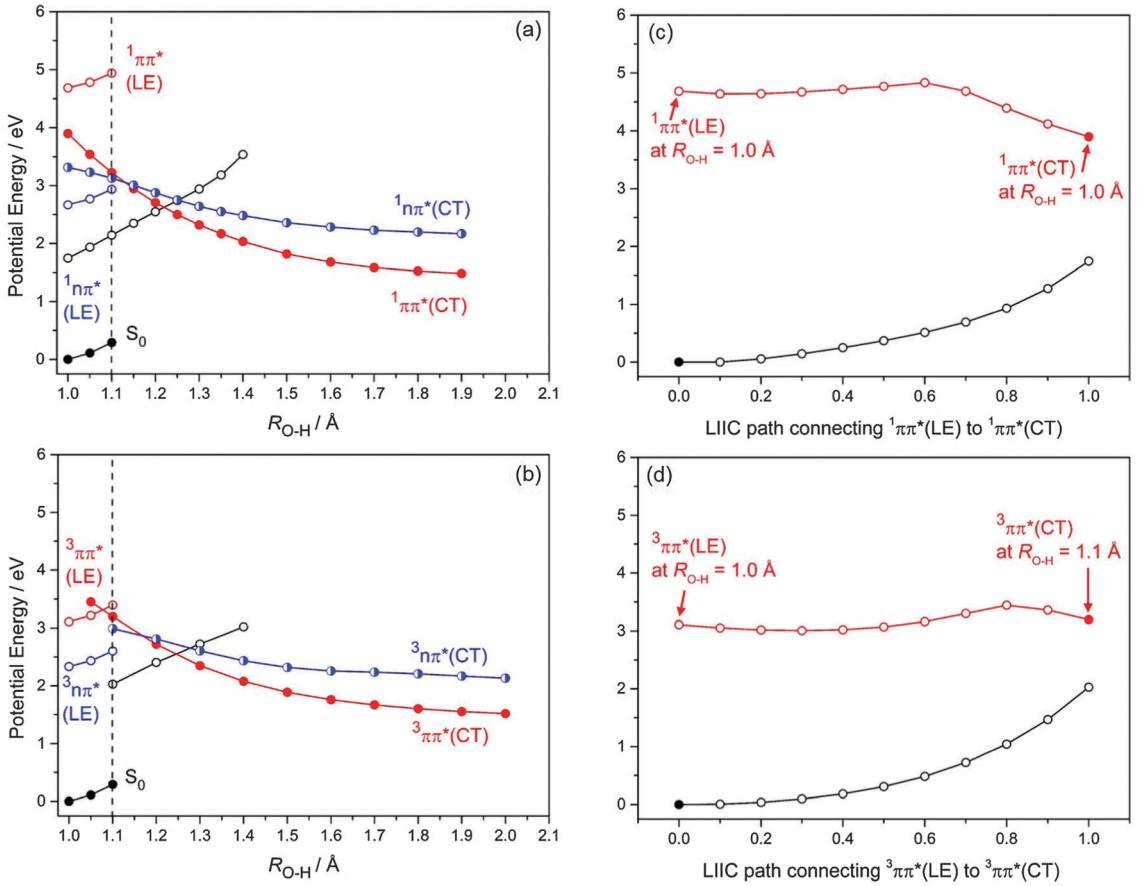

Fig. 3 PE profiles of the ground state and the lowest (a) singlet and (b) triplet excited states of the BQ–H_2O complex along minimum-energy reaction paths for hydrogen transfer from the H_2O molecule to BQ. The S_0 energy along the S_0-optimized reaction path is given by the full black circles. The open coloured circles to the left of the vertical dashed line represent the locally excited (LE) excited states of the BQ chromophore. The energy of the ππ* state of charge-transfer character along the reaction path optimized in this state is given by the full red circles. The half-filled blue circles and open black circles represent, respectively, the energies of the nπ*(CT) state and the S_0 state calculated along the ππ*(CT)-optimized reaction path. The energy profiles along the linearly interpolated reaction path leading from the energy minimum of the ^{1}ππ*(LE) state to the ^{1}ππ*(CT) state at R_{O-H} = 1.0 Å is displayed in (c). The energy profiles of the linearly interpolated reaction path connecting the ^{3}ππ*(LE) state at R_{O-H} = 1.0 Å to the ^{3}ππ*(CT) state at R_{O-H} = 1.1 Å is shown in (d). These reaction profiles were computed at the ADC(2) level.

open black and half-filled blue circles, respectively. It should be noted that crossings of energy profiles belonging to different reaction paths are apparent crossings, while crossings of energies belonging to the same reaction path are true crossings (that is, either avoided crossings or conical intersections). The crossings of the ππ*(CT) and nπ*(CT) energies with the S_0 energy (open black circles), for example, are true crossings.

As depicted in Fig. 3(a) and (b), the energies of the nπ* and ππ* excited states are parallel to the energy of the ground state along the S_0-optimized reaction path – implying no significant driving force for intermolecular proton transfer in these locally excited states. The locally excited states in the BQ–H_2O complex are therefore nonreactive with respect to water oxidation. In the singlet and triplet ππ* excited states of CT character an electron is promoted from the oxygen $2p_x$ orbital localised on H_2O to a ring-centred π* orbital (see Fig. 4(a)). In the singlet and triplet nπ* excited states of CT character, an electron is promoted from the $2p_y$ orbital on H_2O to the same π* orbital. The transfer of a proton from H_2O to BQ in the ^{1}ππ*(CT) and ^{1}nπ*(CT) states compensates this charge separation and leads to the pronounced stabilization (by about 2 eV) of the CT states with increasing R_{O-H} seen in Fig. 3(a) and (b). The neutralization of the electronic charge separation in the CT states provides the driving force for the transfer of the proton from H_2O to BQ (electron-driven proton transfer (EDPT)[46]). The energy of the closed-shell electronic ground state, on the other hand, rises steeply along the reaction paths optimized in the singlet and triplet ππ*(CT) states. As a result, the biradical states arising from proton transfer in the charge-separated states drop below the energy of the ground state for $R_{O-H} > 1.3$ Å. They are thus electronically stable species in this region of nuclear coordinate space.

The energy of the ^{1}nπ*(CT) state at R_{O-H} = 1.0 Å is ≈0.6 eV below the optimised energy of the locally excited ^{1}ππ* state, but is ∼0.5 eV above the ^{1}ππ*(CT) state in the product region (at R_{O-H} = 1.4 Å) – due to a smaller gradient of the ^{1}nπ* state along R_{O-H}. This results in a symmetry-allowed ^{1}ππ*(CT)/^{1}nπ*(CT) energy crossing at R_{O-H} = 1.13 Å which becomes a CI when

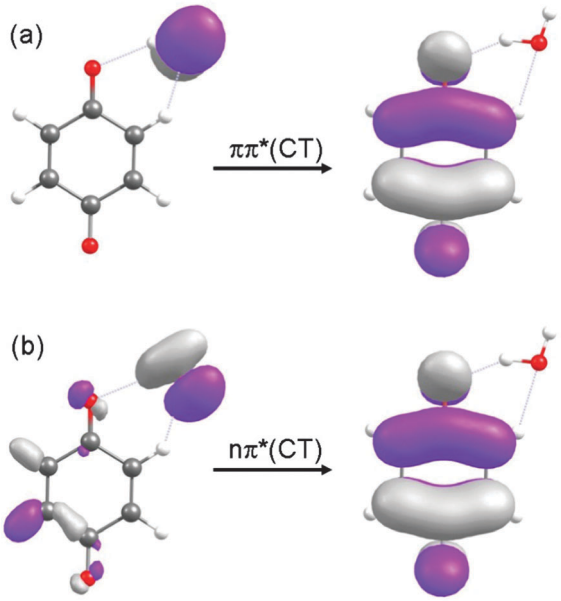

Fig. 4 The molecular orbitals involved in the $^1\pi\pi^*$(CT) and $^1n\pi^*$(CT) states, calculated at R_{O-H} = 1.0 Å, are displayed in (a) and (b), respectively.

displacements along out-of-plane coordinates are considered. The energy crossings of the $^1n\pi^*$(CT) and $^1\pi\pi^*$(CT) states with the S_0 state occur at, respectively, R_{O-H} = 1.25 Å and = 1.22 Å, see Fig. 3(a). While the $^1n\pi^*(A'')/S_0(A')$ energy crossing is symmetry-allowed in C_s symmetry, the $^1\pi\pi^*/S_0$ crossing is an avoided crossing, since both states are of A′ symmetry.

At long range ($R_{O-H} > 1.4$ Å), singlet and triplet states of the ππ* and nπ* biradicals are degenerate – reflecting the vanishing exchange integral for the spatially separated unpaired electrons. A $^3\pi\pi^*(A')/^3n\pi^*(A'')$ symmetry-allowed energy crossing is evident along the proton-transfer path at R_{O-H} = 1.16 Å. At longer R_{O-H}, spin-symmetry allowed crossings of the energies of the $^3\pi\pi^*$ and $^3n\pi^*$ states with the energy of the S_0 are located at R_{O-H} = 1.28 Å and R_{O-H} = 1.24 Å, respectively.

One key difference in the triplet states compared to the singlet states is the relative energy of the locally excited $^3\pi\pi^*$ state in the FC region compared to that of the $^3\pi\pi^*$(CT) state, see Fig. 3(a) and (b). The locally excited $^3\pi\pi^*$ state is below the energy of the $^3\pi\pi^*$(CT) state at short R_{OH} distances – implying the existence of a potential barrier *en route* to intermolecular hydrogen transfer.

To explore the accessibility of the $^1\pi\pi^*$(CT) state from the energy minimum of the locally excited $^1\pi\pi^*$ state of BQ, the energy profile of the $^1\pi\pi^*$ state was computed along the linearly interpolated path connecting the minimum of the $^1\pi\pi^*$(LE) surface with $^1\pi\pi^*$(CT) energy at R_{O-H} = 1.0 Å. As depicted in Fig. 3(c), this energy profile exhibits a low barrier of about 0.25 eV. We emphasize that this represents an upper limit to the actual barrier height, since this linearly interpolated reaction path is not a minimum-energy path. The true minimum-energy path connecting the $^1\pi\pi^*$(LE) and $^1\pi\pi^*$(CT) states is most likely barrierless. The corresponding profile of the $^3\pi\pi^*$ state exhibits a somewhat higher barrier, due to the lower energy of the locally excited $^3\pi\pi^*$ state, see Fig. 3(d).

As Fig. 3(a) shows, the vertically excited $^1\pi\pi^*$(LE) state is located energetically well above the optimized $^1\pi\pi^*$(CT) state at R_{O-H} = 1.0 Å. In addition, Fig. 3c indicates a negligible barrier (if any) on the reaction path from the $^1\pi\pi^*$(LE) state to the $^1\pi\pi^*$(CT) state. We therefore expect a rapid transition from the locally-excited $^1\pi\pi^*$ state to the charge-transfer state upon vertical excitation of the BQ–H_2O complex, followed by ultrafast proton transfer and formation of the BQH•–OH• biradical product. *En route*, branching of the population of the $^1\pi\pi^*$(CT) state to the $^1n\pi^*$ and S_0 states may occur at the various energy crossings described above.

ISC may also occur following vertical excitation to the locally excited $^1\pi\pi^*$ state – the energy of which far exceeds the energy of the relaxed $^3\pi\pi^*$(CT) state. In this case, proton transfer in the $^3\pi\pi^*$(CT) state may lead to the formation of the triplet BQH•–OH• biradical. The excess energy becoming available after proton-transfer in the singlet or triplet states (about 2 eV) is substantial and by far sufficient to dissociate the BQH•–OH• biradical, leading to free BQH• and OH• radicals.

3.4 Photodetachment of H-atoms from semiquinone and hydroquinone

3.4.1 Ground state structures, vertical excitation energies and oscillator strengths. Hydrogenation of BQ at a single O acceptor site leads to the formation of the semiquinone (BQH•) radical. Disproportionation of two BQH• radicals is exoergic and leads to the formation of BQ and the fully hydrogenated species hydroquinone (BQH_2). Hence the H-atom photodetachment reactions of both species have been studied. The ground-state equilibrium structures of BQH• and BQH_2 are displayed in Fig. 5.

Listed in Table 2 and depicted in Fig. 6 are, respectively, the vertical excitation energies of various low-lying electronic states and the orbital promotions involved in forming the low-lying excited electronic states of BQH• and BQH_2.

(A) Semiquinone (BQH•). The BQH• radical is an open-shell species with a single electron in a ring-centred π orbital – *i.e.* in the 5a″ singly occupied molecular orbital (SOMO), see Fig. 6(a). The equilibrium geometry of the ground-state BQH• radical is

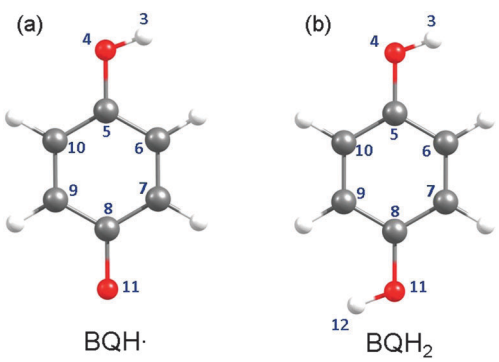

Fig. 5 Structures of the BQH• radical (left) and the BQH_2 molecule (right). When applicable, the atomic numbering assigned to each structure will be referred to in the main text.

Table 2 Vertical excitation energies and oscillator strengths (in parentheses) of BQH• and BQH_2

	Vertical excitation energy/eV	
State	CASSCF/aug-cc-pVDZ	CASPT2/aug-cc-pVDZ
Semiquinone		
$^2n\pi$	0.71 (3.3×10^{-8})	0.90
$^2\pi\pi$	3.09 (4.1×10^{-7})	2.75
$^2\pi\pi^*$	4.90 (1.9×10^{-6})	4.80
$^2\pi\sigma^*$	4.94 (0.0001)	4.89
Hydroquinone		
$^1\pi\pi^*$	4.63 (0.0306)	4.17
$^1\pi\sigma^*$	5.17 (0.0009)	5.00

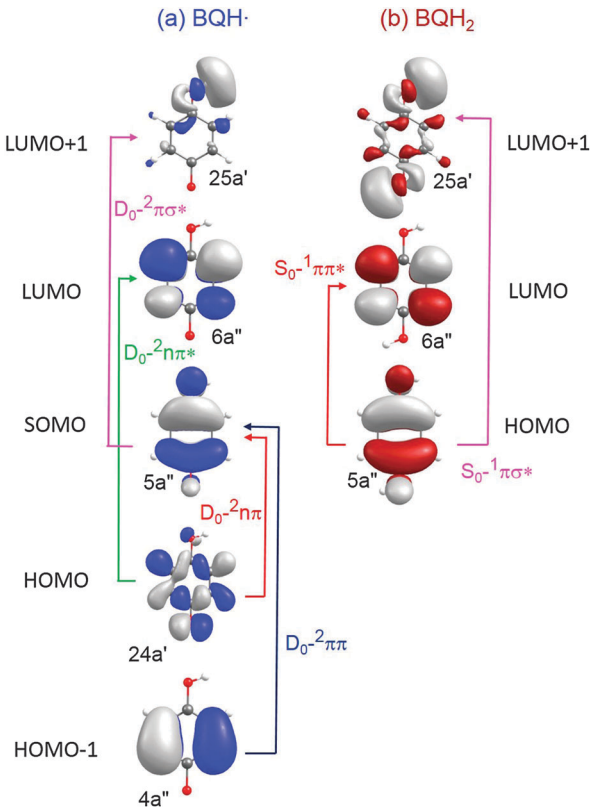

Fig. 6 CASSCF orbitals and orbital promotions of the low-energy excited electronic states of BQH• and BQH_2.

planar (Fig. 5(a)). The planar geometry at the C6C5O4H3 dihedral angle can be understood by recognising that the O–H group is a strong π donor and that the O($2p_x$) orbital undergoes substantial conjugation with the ring π system.

Upon vertical excitation, the lowest-lying excited states are, in the order of increasing energy, $^2n\pi$, $^2\pi\pi$, $^2\pi\pi^*$ and $^2\pi\sigma^*$. The $^2n\pi$ and $^2\pi\pi$ electronic states involve the electron promotions SOMO ← HOMO and SOMO ← HOMO−1, respectively (see Fig. 6). In each case, the SOMO and HOMO−1 are ring centred π orbitals and the HOMO is the O($2p_y$) non-bonding orbital. The CASPT2 excitation energies of the $^2n\pi$ and $^2\pi\pi$ electronic states are, respectively, 0.90 eV and 2.75 eV (see Table 2), placing the absorption maxima of these states in the near infrared and visible regions, respectively. These two states are, however, essentially dark. The $^2n\pi^*$ and $^2\pi\sigma^*$ states arise from, respectively, LUMO ← HOMO and LUMO+1 ← SOMO excitations. The LUMO is a ring-centred π^* orbital, whereas the LUMO+1 is the σ^* orbital localised on the O–H bond (25a′). The CASPT2 vertical excitation energies of the $^2\pi\pi^*$ and $^2\pi\sigma^*$ states are very similar, 4.80 eV and 4.89 eV, respectively, and they carry very little oscillator strength (see Table 2).

(B) Hydroquinone (BQH_2). The ground-state equilibrium geometry of BQH_2 is planar (C_s symmetry). Rotational isomerism of the O–H moieties leads to two distinct, but energetically similar, *syn* and *anti* conformations – predicting equal Boltzmann populations of both rotamers at 298 K. For brevity, the following discussion exclusively refers to the *anti* isomer.

In the FC region, two low-lying electronic states, of $^1\pi\pi^*$ and $^1\pi\sigma^*$ nature, exist in the near-UV. The predicted energetic ordering, $^1\pi\pi^* < {}^1\pi\sigma^*$, is in agreement with analogous systems such as phenol, 4-methoxyphenol and catechol.[41–44] Formation of the $^1\pi\pi^*$ state involves a LUMO ← HOMO electron promotion (Fig. 6(b)). The participating orbitals show good spatial overlap, which is reflected in significant oscillator strength of this transition (Table 2). The vertical excitation energy of the $^1\pi\pi^*$ state is 4.20 eV at the CASPT2 level. ADC(2) predicts 4.60 eV. Both levels of theory predict the S_1–S_0 excitation of BQH_2 to lie in the near UV region. The experimentally derived S_1–S_0 origin line is 4.15 eV (of the *anti* rotamer), measured *via* jet-cooled 1 + 1 resonance enhanced multiphoton ionisation (REMPI) spectroscopy.[45] The REMPI spectrum also reveals a select subset of Franck–Condon active vibrations. All of these lines are much less intense than the electronic origin band, which indicates that the S_0 and S_1 states have similar equilibrium geometries in all nuclear coordinates. At higher vertical excitation energies, CASPT2 predicts the presence of a $^1\pi\sigma^*$ state, the energy of which is calculated to be 5.00 eV. This electronic state arises from a σ^* ← HOMO electron promotion (Fig. 6(b)) and carries a very low oscillator strength (Table 2).

3.4.2 Hydrogen-detachment reaction path. In photoinduced water splitting with the BQ chromophore (as described above), the water–oxidation reaction (eqn (1)) must be followed by the release of a hydrogen atom from BQH• by a second photon (eqn (2)). To explore the feasibility of this reaction, the PE profiles (rigid scans) of BQH• and BQH_2 along the hydrogen-detachment (O–H bond fission) coordinate were calculated and are displayed in Fig. 7(a) and (b), respectively. Previous calculations for similar systems showed that the PE profiles of rigid scans are very similar to those of relaxed scans.[42,46]

(A) Semiquinone (BQH•). BQH• is an exemplar of hypervalent aromatic radicals, the photochemistries of which have thus far received relatively little attention – due to the experimental challenges in preparing such species. Fig. 7(a) presents the PE profiles of the lowest five doublet states of BQH• along the R_{O-H} bond-extension coordinate. Along this coordinate, the D_0, $^2n\pi$, $^2\pi\pi$ and $^2\pi\pi^*$ states are all bound, while the $^2\pi\sigma^*$ state is dissociative with respect to O–H bond elongation. In the FC

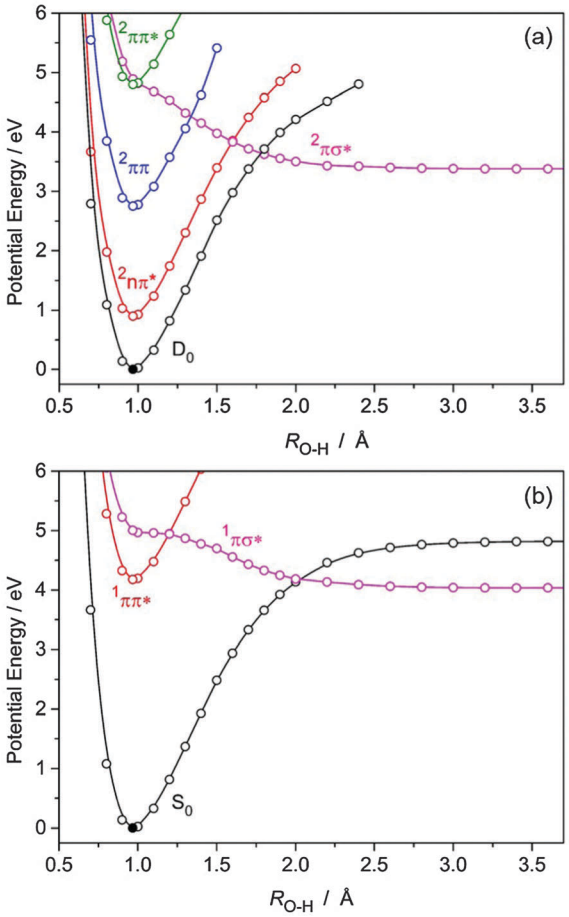

Fig. 7 PE profiles of (a) $BQH^\bullet$ and (b) BQH_2, computed along the R_{O-H} hydrogen detachment coordinate at the CASPT2/aug-cc-pVDZ level.

region, the $^2\pi\sigma^*$ state exhibits oxygen 3s Rydberg character, which develops progressively O–H centered σ* valence character upon bond extension. The $^2\pi\sigma^*$ state predissociates the second $^2\pi\pi^*$ state near the minimum of the latter. The $^2\pi\sigma^*$ state correlates asymptotically with BQ in its ground state and an $H^\bullet$ atom. The calculated bond dissociation energy is $D_e[BQH \rightarrow BQ + H] = 3.38$ eV and is lower than the bond dissociation energy of the D_0 state (see Fig. 7(a)). The crossings of the $^2\pi\sigma^*(A')$ and $^2\pi\pi^*(A'')$ energies are symmetry-allowed in C_s symmetry, but become conical intersections when out-of-plane vibrational modes are taken into account. Following electronic excitation to the second $^2\pi\pi^*$ state, a nonadiabatic transition to the $^2\pi\sigma^*$ state can occur *via* nonadiabatic coupling at the $^2\pi\pi^*/^2\pi\sigma^*$ CI – which is expected to be ultrafast, given that the $^2\pi\pi^*$ and $^2\pi\sigma^*$ states are essentially degenerate in the FC region.

Following the $^2\pi\pi^* \rightarrow {}^2\pi\sigma^*$ nonadiabatic transition, the wave packet in the dissociative $^2\pi\sigma^*$ state encounters three further CIs with the $^2\pi\pi$, $^2n\pi$ and S_0 states. At these CIs, internal conversion from the $^2\pi\sigma^*$ state to the $^2\pi\pi$, $^2n\pi$ and D_0 states may occur – the efficiencies of which will depend on the strength of the nonadiabatic couplings and on the local topographies of the PE surfaces at these CIs. Photodetachment of the H-atom requires that the wave packet in the $^2\pi\sigma^*$ state crosses the $^2\pi\pi$, $^2n\pi$ and D_0 states diabatically. Since there is a dearth of experimental data on the photodissociation dynamics of heterocyclic aromatic radicals and since such data are not likely to become available any time soon, *ab initio* based nonadiabatic quantum dynamics calculations or quasi-classical trajectory surface-hopping simulations have to be performed in order to estimate the quantum yield of photoinduced H-atom formation from $BQH^\bullet$. At somewhat higher excitation energies, direct (or vibronically induced) excitation to the nearly dark $^2\pi\sigma^*$ state could occur and has been previously postulated in related molecules.[44,47–49] In this case, prompt O–H bond fission is expected to occur within tens of femtoseconds (by analogy with phenol),[41] although the role of the $^2\pi\sigma^*/^2\pi\pi^*$ and $^2\pi\sigma^*/^2n\pi^*$ CIs in $BQH^\bullet$ is unknown.

(B) Hydroquinone (BQH_2). In this sub-section, we discuss the photochemistry of the closed-shell BQH_2 molecule in order to compare and contrast its photochemistry with that of the $BQH^\bullet$ radical. The discussion of the photochemistry of BQH_2 and the comparisons drawn with $BQH^\bullet$ benefit greatly from the multitude of available experimental and theoretical data for phenolic molecules (phenol, 4-methoxyphenol, hydroquinone, *etc.*) – which are lacking for the open-shell analogues such as $BQH^\bullet$.

Fig. 7(b) presents the PE profiles of the lowest three singlet states of BQH_2 along the R_{O-H} bond extension coordinate. The situation in BQH_2 is much the same as in phenol or catechol, *i.e.* the $^1\pi\pi^*$ state is bound and is predissociated by a $^1\pi\sigma^*$ state, which is repulsive along the O–H bond extension coordinate and asymptotically correlates with $BQH^\bullet + H^\bullet$ products. As such, BQH_2 should undergo O–H bond fission following near-UV excitation to the bright $^1\pi\pi^*$ state – the efficiency of which will depend on the extent to which the $^1\pi\pi^*$ and $^1\pi\sigma^*$ states are nonadiabatically coupled. The energy of the $^1\pi\sigma^*/^1\pi\pi^*$ crossing relative to the $^1\pi\pi^*$ minimum is higher than in the $BQH^\bullet$ radical, see Fig. 7. Following electronic excitation to the onset of the $^1\pi\pi^*$ state, nonadiabatic tunneling along the O–H coordinate beneath the barrier created by the $^1\pi\pi^*/^1\pi\sigma^*$ CI is required for population of the dissociative $^1\pi\sigma^*$ state – followed by prompt O–H bond fission. In phenol, the equivalent tunneling lifetime has been measured to be ~2 ns for the lowest vibrational level.[51] It decreases sharply when higher vibrational levels are excited.[41] Analogous with phenol, direct or vibronically induced population of the $^1\pi\sigma^*$ state in BQH_2 will drive ultrafast (sub-50 fs) O–H bond fission at elevated photon energies – yielding the asymptotic $BQH^\bullet + H^\bullet$ products with a calculated $D_e[BQH_2 \rightarrow BQH^\bullet + H]$ of 4.04 eV. The difference in D_e of $BQH^\bullet$ and BQH_2 can be understood by recognising that the $BQH^\bullet \rightarrow BQ + H$ photoreaction forms the closed-shell BQ molecule. In contrast, the $BQH_2 \rightarrow BQH^\bullet + H^\bullet$ photo-reaction forms the chemically less stable open-shell $BQH^\bullet$ radical.

4. General discussion and conclusions

Ab initio electronic-structure calculations have been used to explore the photoinduced proton-transfer reaction in the BQ–H_2O complex (photoreaction (1)) and the hydrogen photodetachment from the $BQH^\bullet$ radical that may occur thereafter (photoreaction (2)).

Since semiquinone radicals disproportionate spontaneously to yield BQ and BQH_2, the photodetachment of H-atoms could also occur from the latter. We have characterised the minimum-energy pathways connecting the well-known locally excited spectroscopic states of the BQ chromophore to hitherto unknown charge-separated excited states in both the singlet and triplet spin multiplicities of the BQ–H_2O hydrogen-bonded complex. These results clarify controversial key questions concerning the nature of the reactive electronic states involved in the photoreactivity of BQ in aqueous solution. We have provided insights into the mechanisms by which BQ is capable of photo-oxidation of water – which is the initiation step for water splitting with an aromatic photobase (photoreaction (1)).

Photoreaction (1) involves initial excitation to a locally excited singlet electronic state ($^1\pi\pi^*$(LE)) the PE surface of which is adiabatically connected in a barrierless manner to the PE surface of a dark charge-separated singlet electronic state. Following the transition from the $^1\pi\pi^*$(LE) state to the $^1\pi\pi^*$(CT) state, the transfer of the proton from the H_2O molecule to BQ neutralizes the electronic charge separation, which results in a substantial energetic stabilisation of the electronic CT states which become neutral biradical states. Since the closed-shell ground state is strongly destabilized by the proton transfer, the $^1\pi\pi^*$ and $^1n\pi^*$ biradical product states are lower in energy than the electronic ground state at the equilibrium geometry of the latter (Fig. 3(a)). Importantly, the products of these excited-state electron/proton transfer reactions are radical pairs rather than ion pairs (which are formed in ground-state proton-transfer reactions). The non-adiabatic transitions between the various electronic states are governed by avoided crossings or CIs. At the energy crossings of the biradical states with the S_0 state, the reaction bifurcates into either (i) formation of biradicals or (ii) internal conversion to the electronic ground state, followed by re-formation of the original complex after vibrational energy relaxation.

The LE and CT states in the triplet manifold of the BQ–H_2O complex exhibit essentially identical PE profiles along the hydrogen-transfer coordinate as in the singlet manifold. While photoexcitation of the BQ–H_2O complex leads to the population of singlet excited states, triplet excited states can be populated when ISC competes effectively with the reaction and relaxation processes in the singlet manifold. The $^3\pi\pi^*$(CT)/S_0 and $^3n\pi^*$(CT)/S_0 intersections represent allowed crossings to a very good approximation, since the spin–orbit coupling is weak. Therefore, flux evolving on the $^3\pi\pi^*$(CT) state will continue *en route* to forming the biradical species with little or no perturbation by the electronic ground-state PE surface. The absence of electronic inter-state transitions at the $^3\pi\pi^*$(CT)/S_0 and $^3n\pi^*$(CT)/S_0 intersections will likely lead to an enhanced yield of biradical products compared to the singlet manifold.

The $BQH^\bullet$ radical formed in photoreaction (1) may either serve as a reducing agent or the surplus H-atom may be photodetached *via* photoreaction (2). A repulsive $^2\pi\sigma^*$ state is predicted to exist in the near-UV excitation region which may provide a channel for direct and fast H-atom photodetachment. Analogous $^1\pi\sigma^*$ states in phenol are known to yield H-atom photoproducts.[41] $BQH^\bullet$ features, however, low-lying bound $^2\pi\pi$ and $^2n\pi$ states, which are intersected by the $^2\pi\sigma^*$ state *en route* to O–H bond fission. These additional energy crossings may cause trapping of the population of the $^2\pi\sigma^*$ state *via* internal conversion – reducing the quantum yield of BQ + H photoproducts. The probability of IC to the $^2\pi\pi$ and $^2n\pi$ states will depend on the strength of the non-adiabatic coupling at the various CIs along the $^2\pi\sigma^*$ state. These issues require further investigation by electronic-structure and quantum dynamics calculations.

We note that $BQH^\bullet$ is only partially reduced and contains a free carbonyl oxygen which is available for the oxidation of another H_2O molecule *via* excited-state hydrogen abstraction. Following photoexcitation by a second photon, the O–H bond fission channel described above may compete with the $BQH^\bullet$–$H_2O + h\nu \rightarrow BQH_2 + OH^\bullet$ photoreaction involving another water molecule. The relative branching into H-atom abstraction from water or H-atom photodetachment from $BQH^\bullet$ will depend on the energetics of the second H-atom abstraction process. These questions are beyond the scope of the present study, but deserve future investigation.

An important feature evidenced by the present work is that the excited-state electron/proton-transfer process in BQ–H_2O is exoergic and most likely barrierless, which is not the case in the pyridine–water (Py–H_2O) complex, for example, for which a potential barrier of 0.23 eV for H-atom transfer from the H_2O molecule to pyridine has been predicted at the ADC(2) level.[3] We therefore expect that photo-induced proton transfer occurs on a faster timescale and with higher efficiency in the BQ–H_2O complex than in the pyridine–H_2O complex. On the other hand, the H-atom photodetachment from the $BQH^\bullet$ radical involves curve crossings with three bound electronic states along the O–H bond elongation coordinate, which may reduce the H-atom yield.

BQ, like pyridine, absorbs in the UV and, as such, is not a suitable photocatalyzer for solar water splitting. Moreover, the oscillator strengths of the $^1\pi\pi^*$ transitions in the BQ–H_2O complex are extremely small, since these transitions are dipole-forbidden in the isolated BQ chromophore. The $D_0 \rightarrow {}^1\pi\pi^*$ transitions in the $BQH^\bullet$ radical likewise are in the UV and exhibit very low oscillator strengths. Therefore, the BQ–H_2O complex should be considered as an idealized model system which is suitable for the investigation of the fundamental mechanisms of the coupled electron/proton transfer reactions involved in photoinduced water splitting. The small size of this complex allows the application of relatively accurate first-principles computational methods, including forthcoming quantum mechanical or quasi-classical simulations of the excited-state reaction dynamics. Practically suitable photoactive chromophores should absorb in the visible (or more precisely, within the range of the solar spectrum that reaches the surface of earth) with substantial oscillator strengths. Once the mechanistic details of the electron/proton coupled reactions in the photo-excited BQ–H_2O complex are understood, the next logical step will be the systematic engineering of the quinone chromophore, say A, to optimize its functionality as a photocatalyst for solar water splitting. Relative to BQ, such improvements should involve (i) a shift of the absorption maximum of the chromophore A to longer wavelengths (to within the visible spectrum) by

extension of the π-conjugated system, (ii) optimisation of the oscillator strength of A in order to maximise the absorption efficiency, (iii) ensuring low energetic barriers separating the locally excited states and the CT states that drive the proton transfer in the A–H_2O complex and (iv) lowering the absorption maximum of the $AH^{\bullet}$ radical whilst maximising its absorption efficiency. Possible candidates which may encompass all or at least some of the above requirements are anthraquinone dyes. These exhibit an extended π-conjugation that leads to a bathochromic shift of the absorption maximum. The singlet ππ* excited electronic states of anthraquinone dyes are electric-dipole allowed and exhibit large absorption cross sections in the visible region, rendering these dyes promising candidates as photocatalyzers for solar water splitting.

A potential drawback of quinones as water-splitting catalysts is the rather high dissociation threshold of the reduced species, as indicated by the calculated dissociation energies of 3.38 eV for $BQH^{\bullet}$ and 4.04 eV for BQH_2. This fact is related, of course, to the exceptionally high oxidation potential of photoexcited BQ and implies that near-UV photons are required to drive the photodissociation of $BQH^{\bullet}$ or BQH_2. For comparison, the calculated dissociation energies of the pyridinyl and acridinyl radicals are 1.7 eV and 3.0 eV, respectively.[2,4] However, judicious substitution with π-donating groups (such as NH_2 or OMe) has previously been shown to greatly reduce the bond dissociation energy of phenol[50] – which, to first order, should translate to BQ and anthraquinones, thus lowering the threshold for photoreaction (2).

Acknowledgements

The authors are grateful to Xiaojun Liu and Andrzej Sobolewski for fruitful discussions. T.N.V.K. thanks the Technical University of Munich for a post-doctoral research fellowship. D.T. is grateful for a Ph.D. fellowship granted by the International Max Planck Research School of Advanced Photon Science (IMPRS-APS) and for support by the TUM Graduate School. W.D. thanks the Deutsche Forschungsgemeinschaft for support *via* the Munich Centre for Advanced Photonics.

References

1 B. Loll, J. Kern, W. Saenger, A. Zouni and J. Biesiadka, *Nature*, 2005, **438**, 1040–1044.
2 X. Liu, A. L. Sobolewski, R. Borelli and W. Domcke, *Phys. Chem. Chem. Phys.*, 2013, **15**, 5957–5966.
3 X. Liu, A. L. Sobolewski and W. Domcke, *J. Phys. Chem. A*, 2014, **118**, 7788–7795.
4 X. Liu, A. L. Sobolewski and W. Domcke, *J. Phys. Chem. B*, 2015, **119**, 10664–10672.
5 T.-K. Yang and C.-Y. Shen, *Encyclopedia of Reagents for Organic Synthesis*, John Wiley & Sons, Ltd, 2001.
6 M. Oda, T. Kawase, T. Okada and T. Enomoto, *Org. Synth.*, 1996, **73**, 253.
7 S. M. Beck and L. E. Brus, *J. Am. Chem. Soc.*, 1982, **104**, 1103–1104.
8 S. M. Beck and L. E. Brus, *J. Am. Chem. Soc.*, 1982, **104**, 4789–4792.
9 A. I. Ononye, A. R. McIntosh and J. R. Bolton, *J. Phys. Chem.*, 1986, **90**, 6266–6270.
10 K. C. Kurien and P. A. Robins, *J. Chem. Soc. B*, 1970, 855–859.
11 A. E. Alegria, A. Ferrer and E. Sepulveda, *Photochem. Photobiol.*, 1997, **66**, 436–442.
12 T. Matsumoto, M. Sato and S. Hirayama, *Chem. Phys. Lett.*, 1973, **18**, 563–566.
13 R. E. Connors and W. R. Christian, *J. Phys. Chem.*, 1982, **86**, 1524–1528.
14 A. Pochon, P. P. Vaughan, D. Gan, P. Vath, N. V. Blough and D. E. Falvey, *J. Phys. Chem. A*, 2002, **106**, 2889–2894.
15 C. F. Wells, *Trans. Faraday Soc.*, 1961, **57**, 1703–1718.
16 B. Atkinson and M. Di, *Trans. Faraday Soc.*, 1958, **54**, 1331–1339.
17 C. F. Wells, *Nature*, 1956, **177**, 483–484.
18 J.-C. Ronfard-Haret, R. V. Bensasson and E. Amouyal, *J. Chem. Soc., Faraday Trans. 1*, 1980, **76**, 2432–2436.
19 J. N. Moore, D. Phillips and R. E. Hester, *J. Phys. Chem.*, 1988, **92**, 5619–5627.
20 S. Perun, A. L. Sobolewski and W. Domcke, *J. Phys. Chem. A*, 2006, **110**, 9031–9038.
21 A. L. Sobolewski, W. Domcke and C. Hättig, *Proc. Natl. Acad. Sci. U. S. A.*, 2005, **102**, 17903–17906.
22 A. L. Sobolewski and W. Domcke, *J. Phys. Chem. A*, 2001, **105**, 9275–9283.
23 M. Barbatti, A. J. A. Aquino, J. J. Szymczak, D. Nachtigallová, P. Hobza and H. Lischka, *Proc. Natl. Acad. Sci. U. S. A.*, 2010, **107**, 21453–21458.
24 S. Clifford, M. J. Bearpark, F. Bernardi, M. Olivucci, M. A. Robb and B. R. Smith, *J. Am. Chem. Soc.*, 1996, **118**, 7353–7360.
25 W. Domcke, D. R. Yarkony and H. Köppel, *Conical Intersections: Electronic Structure, Dynamics and Spectroscopy*, World Scientific, Singapore, 2004.
26 W. Domcke, D. R. Yarkony and H. Köppel, *Conical Intersections: Theory, Computation and Experiment*, World Scientific, Singapore, 2011.
27 M. Klessinger and J. Michl, *Excited States and Photochemistry of Organic Molecules*, Wiley-VCH, Weinheim, 1995.
28 C. Møller and M. S. Plesset, *Phys. Rev.*, 1934, **46**, 618–622.
29 T. H. Dunning, Jr., *J. Chem. Phys.*, 1989, **90**, 1007–1023.
30 B. O. Roos, P. A. Malmqvist, V. Molina, L. Serrano-Andres and M. Merchan, *J. Chem. Phys.*, 2002, **116**, 7526–7536.
31 A. Dreuw and M. Wormit, *Wiley Interdiscip. Rev.: Comput. Mol. Sci.*, 2015, **5**, 82–95.
32 *TURBOMOLE V6.4 2012*, a development of University of Karlsruhe and Forschungszentrum Karlsruhe GmbH, 1989–2007, TURBOMOLE GmbH, since 2007, available from www.turbomole.com.
33 H. J. Werner, P. J. Knowles, G. Knizia, F. R. Manby, M. Schütz, P. Celani, T. Korona, R. Lindh, A. Mitrushenkov, G. Rauhut,

K. R. Shamasundar, T. B. Adler and R. D. Amos, *et al.*, *MOLPRO*, University of Cardiff, Cardiff, U.K., 2010.
34 G. Ter Horst and J. Kommandeur, *Chem. Phys.*, 1979, **44**, 287–293.
35 R. Pou-Amérigo, M. Merchán and E. Ortí, *J. Chem. Phys.*, 1999, **110**, 9536–9546.
36 J. Weber, K. Malsch and G. Hohlneicher, *Chem. Phys.*, 2001, **264**, 275–318.
37 Y. Honda, M. Hada, M. Ehara and H. Nakatsuji, *J. Phys. Chem. A*, 2002, **106**, 3838–3849.
38 M. Schreiber, M. R. Silva-Junior, S. P. A. Sauer and W. Thiel, *J. Chem. Phys.*, 2008, **128**, 134110.
39 M. R. Silva-Junior, M. Schreiber, S. P. A. Sauer and W. Thiel, *J. Chem. Phys.*, 2010, **133**, 174318.
40 P. H. P. Harbach, M. Wormit and A. Dreuw, *J. Chem. Phys.*, 2014, **141**, 064113.
41 A. Iqbal, L.-J. Pegg and V. G. Stavros, *J. Phys. Chem. A*, 2008, **112**, 9531–9534.
42 T. N. V. Karsili, A. M. Wenge, B. Marchetti and M. N. R. Ashfold, *Phys. Chem. Chem. Phys.*, 2014, **16**, 588–598.
43 G. A. King, A. L. Devine, M. G. D. Nix, D. E. Kelly and M. N. R. Ashfold, *Phys. Chem. Chem. Phys.*, 2008, **10**, 6417–6429.
44 O. P. J. Vieuxmaire, Z. Lan, A. L. Sobolewski and W. Domcke, *J. Chem. Phys.*, 2008, **129**, 224307.
45 N. Biswas, S. Chakraborty and S. Wategaonkar, *J. Phys. Chem. A*, 2004, **108**, 9074–9081.
46 A. L. Sobolewski and W. Domcke, *J. Phys. Chem. A*, 2007, **111**, 11725–11735.
47 M. G. D. Nix, A. L. Devine, B. Cronin and M. N. R. Ashfold, *Phys. Chem. Chem. Phys.*, 2006, **8**, 2610–2618.
48 M. G. D. Nix, A. L. Devine, B. Cronin, R. N. Dixon and M. N. R. Ashfold, *J. Chem. Phys.*, 2006, **125**, 133318.
49 A. L. Devine, M. G. D. Nix, R. N. Dixon and M. N. R. Ashfold, *J. Phys. Chem. A*, 2008, **112**, 9563–9574.
50 T. N. V. Karsili, A. M. Wenge, S. J. Harris, D. Murdock, J. N. Harvey, R. N. Dixon and M. N. R. Ashfold, *Chem. Sci.*, 2013, **4**, 2434–2446.
51 G. M. Roberts, A. S. Chatterley, J. D. Young and V. G. Stavros, *J. Phys. Chem. Lett.*, 2012, **3**, 348–352.
52 J. Goodman and L. E. Brus, *J. Chem. Phys.*, 1978, **69**, 1604.